*Research Paper*
*Computational Methods for Differential Equations*
http://cmde.tabrizu.ac.ir
Vol. *, No. *, *, pp. 1-21
DOI:10.22034/cmde.2025.65322.2996

# Physical interpretation of exact soliton solutions in the nonlinear Jaulent-Miodek hierarchy equation

**Md Alamgir Hossain[1], Md. Nur Alam[2,3,*], Md. Farhad Hossain[3], Md. Ariful Islam[4], Mohammad Hassan[5], and Cemil Tunç[6,*]**

[1]Department of Mathematics, Govt. Edward College, Pabna-6600, Bangladesh.

[2]Department of Mathematics, Saveetha School of Engineering, Saveetha Institute of Medical and Technical Sciences, Chennai 602105, Tamilnadu, India.

[3]Department of Mathematics, Pabna University of Science and Technology, Pabna-6600, Bangladesh.

[4]General Education Department, City University, Khagan, Birulia, Savar, Dhaka-1340, Bangladesh.

[5]Department of Mathematics and Scientific Computing, Madan Mohan Malaviya University of Technology, Gorakhpur, U.P. India 273010.

[6]Department of Mathematics, Faculty of Sciences, Van Yuzuncu Yil University, 65080, Van, Turkey.



**Abstract**

This study looks at what exact soliton solutions (ESSs) mean in the nonlinear Jaulent-Miodek Hierarchy (NLJMH) equation, which is important because of its energy-related Schrödinger potential and its uses in areas like optics, physics, soliton theory, geophysics, fluid dynamics, signal processing, plasma physics, and condensed matter physics. Solitons, as fundamental nonlinear wave structures, perform a crucial role in understanding the dynamic behavior of complex systems that are governed by the NLJMH equation. Through rigorous mathematical analysis and symbolic computation techniques, we uncover a range of ESSs, including periodic traveling waves, bright and dark solitons, kink solitons, and their combinations. Each soliton type manifests distinct physical characteristics and behaviors, influencing various phenomena in nonlinear sciences and beyond. Our investigation focuses on elucidating the underlying physical significance of these soliton solutions. By analyzing their profiles, velocities, and interactions, we aim to provide insights into how these nonlinear waves propagate, interact, and impact physical structures. This research contributes to advancing the theoretical comprehension of soliton dynamics within the NLJMH equation framework, highlighting their relevance in fields such as fluid dynamics, plasma physics, optical fibers, and other areas where nonlinear wave phenomena are prevalent. The systematic application of advanced computational tools and rigorous analytical techniques has proven instrumental in uncovering a diverse spectrum of soliton solutions within the NLJMH equation. These findings underscore the method's effectiveness in generating precise and comprehensive insights into complex nonlinear phenomena. The ability to accurately predict and analyze various soliton types, including kink solitons, periodic traveling waves, bright and dark solitons, and their hybrids, showcases the method's robustness and versatility. Based on this study, we can conclude that the process used is highly effective, dependable, productive, and potent for resolving any other nonlinear evolution equations (NLEEs).

**Keywords.** The nonlinear JMH equation, $mG'/GE$, exact soliton solutions, nonlinear evolution equations, nonlinear wave propagation, nonlinear dynamics, Mathematical Physics.

**2010 Mathematics Subject Classification.** 65L05, 34K06, 34K28.

## 1. Introduction

Exact soliton solutions (ESSs) for the nonlinear evolution equations (NLEEs) have been a central area of investigation for the past couple of decades. Applied nonlinear and physical sciences that include telecommunication systems, biology, chemistry, heat and sound transfer, physics, engineering, fluid dynamics, computer science, space systems,

Received: 04 January 2025 ; Accepted: 18 July 2025.
∗ Corresponding authors. Emails: nuralam.pstu23@gmail.com, cemtunc@yahoo.com.

artificial intelligence, population growth, image processing, laser optics, acoustics, plasma and electro mechanics can all benefit from recognizing how to calculate analytical solutions for nonlinear partial differential equations (NLPDEs). Solitons, for instance, may represent shallow-water surface waves, such as tidal bores or tsunamis, in fluid dynamics, contributing to making forecasts of their behavior as well as prospective effects [15]. Solitons are crucial in various fields, particularly in fiber optics, where they help maintain the arrangement of light pulses over extended distances, thereby enhancing data transmission reliability and efficiency [16, 17]. They also play a significant role in understanding stability within fusion reactors and in energy transmission through plasma [37]. Moreover, soliton solutions provide insights into the dynamics of protein folding and the movement of nerve impulses in neurons [18]. Given their importance, developing techniques for finding analytical solutions to NLEEs is vital. However, this task is inherently challenging due to the complexity of NLPDEs. To address these challenges, researchers have developed several analytical strategies, including the modified $mG'/GE$ approach [4–6, 8], the auxiliary equation technique [21], the simplest equation technique [30], the unified approach [22], the SSE approach [10], the F-expansion technique [28], the extended trial equation method [3], Hirota's direct technique [38], the spectral Galerkin technique [23], the SGE procedure [9], the EF method [1], the modify extended auxiliary equation mapping technique [29], Hirota bilinear approach [14], the extended Fan sub-equation approach [36], the Hirota method [34], generalized tanh–coth method [19, 26] and many more. These methods have been instrumental in overcoming obstacles in solving NLPDEs.

The examination of nonlinear dispersive wave events gives rise to the Jaulent-Miodek (JM) hierarchy equations, which are frequently used as models for the propagation of optical pulses in nonlinear media, internal waves in stratified fluids, shallow water waves, and plasma waves. Because dispersion and nonlinearity are perfectly balanced, the soliton solutions in these systems are real, localised energy packets that act like particles. Understanding the nature of these solitons' movements and interactions facilitates understanding the underlying physical systems, such as the stability of signals in nonlinear optical fibres or the conservation of mass and momentum in fluids. The JMH equation is a renowned nonlinear evolution equation (NLEE) with valuable applications across various nonlinear scientific disciplines [33]. It addresses two-dimensional nonlinear physical phenomena, such as wave propagation in physics [24]. This equation was first developed in 1976 by Jaulent and Miodek during their investigation of the relationship between energy-dependent Schrödinger potentials and NLEEs [20]. The JMH equation has been utilized across numerous fields, including enhancing image and signal processing techniques, modeling financial systems with fractional dynamics such as stock market volatility, and designing control systems with fractional derivatives [11]. Additionally, it is employed in the study of optical and plasma systems, viscoelastic materials, and fluid flow phenomena with fractional-order effects [27]. The JMH equation also plays a crucial role in modeling the functioning of biological neurons [7], among other significant phenomena. The investigation of exact soliton solutions (ESSs) for NLEEs is a topic of considerable interest. Numerous researchers have employed various methods to discover the ESSs for the JMH equation. For example, Alzahrani utilized the Optimal auxiliary function method [13], Sahoo and Ray applied both the tanh method and the $mG'/GE$ process [32]. Hu and Qi employed the $\exp(-\phi(z))$-extension process [**?** ], and Akkilic et al. implemented both the $(m+1)/G'(m+1)$-extension procedure and the comprehensive rational sine-cosine process [2]. Additionally, Kaya and Sayed used Adomian's decomposition method [25], Sadat and Kassem applied the integrating factors method [31], Alshammari et al. utilized both the coupled fractional variational iteration and Adomian decomposition transformation techniques [12], and Taha and Noorani also applied the $mG'/GE$ [35], discovering three categories of wave solutions when specific parameter values were considered. In addition to these approaches, numerous other complex methods have been employed to find the ESSs of the JMH equation. In this experiment, we obtained forty ESSs of the JMH equation by applying a $mG'/GE$ process. These solutions have been rigorously analyzed and include kink solitons, periodic traveling waves, anti-kink solitons, bright and dark solitons, and various combinations thereof. Furthermore, we explored the physical structure of eight of these forty solutions, which, to the best of our knowledge, have not been addressed in previous analyses.

To comprehend complex physical processes like wave propagation, energy localisation, and nonlinear interactions in different media, it is crucial to examine accurate soliton solutions in nonlinear evolution equations. The nonlinear Jaulent–Miodek (JM) hierarchy equation provides a complicated mathematical model for explaining dispersive and nonlinear events in fluid dynamics, plasma waves, and nonlinear optics. The physical interpretation of soliton solutions within this hierarchy remains largely unexplored despite its significance. Using the $mG'/GE$ process, the present

research produces new exact solutions and offers an extensive comprehension of their behaviour and physical meaning. The study's value for both theoretical research and practical uses in nonlinear wave dynamics is enhanced by its focus on both mathematical analysis and understanding their physical meaning.

Our paper is organized as follows:

- Section 2 provides an outline of the modified $mG'/GE$ process.
- Section 3 details the formulation of the nonlinear JMH equation.
- Section 4 presents the mathematical analysis and ESSs of the nonlinear JMH equation.
- Section 5 offers the results and discussion, including graphical and physical explanations of the JMH equation.
- Finally, Section 6 concludes the paper.

## 2. Outline of the $mG'/GE$ process

We consider the nonlinear evolution equation (NLEE) taken as follows:

$$Y(W_t, W_x, W_{xx}, W_{yy}, W_{xyxy}, \dots) = 0, \tag{2.1}$$

In Eq. (2.1), $Y$ is a polynomial task for $W(x, y, t)$ and it's all derivatives. Currently we expound the key phases of $mG'/GE$ process.

**Phase 1:** We study that

$$W(x, y, t) = W(\Phi), \quad \Phi = x + y - \omega t, \tag{2.2}$$

Using Eq. (2.2) into Eq. (2.1), then we find:

$$Z(-\omega W', W', W'', W''', \dots) = 0, \tag{2.3}$$

**Phase 2:** The answer for Eq. (2.3) is given as

$$W(\Phi) = \sum_{i=-N}^{N} B_i T^i, \tag{2.4}$$

where $T = \left(\frac{G'}{G} + \frac{\lambda}{2}\right)$, $|B_{-N}| + |B_N| \neq 0$ and $G = G(\Phi)$ fulfills the model

$$G'' + \lambda G' + \mu G = 0, \tag{2.5}$$

where $B_i(\pm 1, \pm 2, \pm 3, \dots, \pm N)$. From Eq. (2.4), we procure

$$T' = s - T^2, \tag{2.6}$$

where $s = \frac{\lambda^2 - 4\mu}{4}$ and $s$ is considered employing $\lambda$ and $\mu$. So, $T$ fulfills the Eq. (2.6) as follows:

$$T = \sqrt{s}\tanh(\sqrt{s}\Phi), \quad s > 0,$$

$$T = \sqrt{s}\coth(\sqrt{s}\Phi), \quad s > 0,$$

$$T = \frac{1}{\Phi}, \quad s = 0,$$

$$T = -\sqrt{-s}\tan(\sqrt{-s}\Phi), \quad s < 0,$$

$$T = \sqrt{-s}\cot(\sqrt{-s}\Phi), \quad s < 0.$$

## 3. ESSs of nonlinear JMH equation

We consider that the JMH equation:

$$U_t + \frac{3}{4}\left(\partial_x^{-1}U_{yy} + U\,\partial_x^{-1}U_y\right) + \frac{1}{2}\left(U_{yy} - 2U^3\right)_x = 0. \tag{3.1}$$

where $\partial_x^{-1}$ is the inverse of $\partial_x$ such that $\partial_x^{-1}\partial_x = \partial_x\partial_x^{-1} = 1$, and $(\partial_x^{-1}g)(x) = \int_{-\infty}^{\infty} g(t)dt$ is called a decaying condition. Let us consider

$$U(x,y,t) = V_x(x,y,t). \tag{3.2}$$

Using (3.2) in (3.1), we find:

$$V_{xt} + \frac{3}{4}V_{xx}V_y + \frac{1}{4}V_{xxxx} + \frac{3}{16}V_{yy} - \frac{3}{2}V_x^2V_{xx} = 0. \tag{3.3}$$

We consider wave transformation as

$$V(x,y,t) = V(\Phi), \quad \Phi = (x+y-\omega t). \tag{3.4}$$

Using (3.4) in (3.3), we find:

$$-\omega V'' + \frac{3}{16}V'' + \frac{3}{4}V''V + \frac{1}{4}V'''' - \frac{3}{4}(V')^2V'' = 0. \tag{3.5}$$

Integrate Eq. (3.5) w. r. to $\Phi$, then we obtain:

$$-16\omega V' + 6(V')^2 + 4V''' + 3V' - 8(V')^3 = 0. \tag{3.6}$$

Let us consider that $V' = W$, then obtain:

$$-16\omega W + 6W^2 + 4W'' + 3W - 8W^3 = 0. \tag{3.7}$$

According to the $mG'/GE$ process, then we get:

$$W(\Phi) = B_{-1}T^{-1} + B_0T^0 + B_1T^1. \tag{3.8}$$

Substituting Eq. (3.8) into Eq. (3.7), we find:

**Case I:**

$$\lambda = \lambda, \quad \mu = \frac{\lambda^2}{4} - \frac{1}{16}, \quad \omega = -\frac{1}{4}, \quad B_0 = \frac{1}{4}, \quad B_1 = 0, \quad B_{-1} = -\frac{1}{16}.$$

Substituting Case I into Eq. (3.8), then we achieve:

$$U_{11}(x,y,t) = -\frac{1}{16}\left(\frac{2}{\sqrt{\lambda^2-4\mu}}\coth\left(\frac{\sqrt{\lambda^2-4\mu}}{2}(x+y-\omega t)\right)\right) + \frac{1}{4}. \tag{3.9}$$

$$U_{12}(x,y,t) = -\frac{1}{16}\left(\frac{2}{\sqrt{\lambda^2-4\mu}}\tanh\left(\frac{\sqrt{\lambda^2-4\mu}}{2}(x+y-\omega t)\right)\right) + \frac{1}{4}. \tag{3.10}$$

$$U_{13}(x,y,t) = -\frac{1}{16}(x+y-\omega t) + \frac{1}{4}. \tag{3.11}$$

$$U_{14}(x,y,t) = -\frac{i}{16}\left(\frac{2}{\sqrt{\lambda^2-4\mu}}\cot\left(i\frac{\sqrt{\lambda^2-4\mu}}{2}(x+y-\omega t)\right)\right) + \frac{1}{4}. \tag{3.12}$$

$$U_{15}(x,y,t) = \frac{i}{16}\left(\frac{2}{\sqrt{\lambda^2-4\mu}}\tan\left(i\frac{\sqrt{\lambda^2-4\mu}}{2}(x+y-\omega t)\right)\right) + \frac{1}{4}. \tag{3.13}$$

**Case II:**

$$\lambda = \lambda, \quad \mu = \frac{\lambda^2}{4} - \frac{1}{16}, \quad \omega = -\frac{1}{4}, \quad B_0 = \frac{1}{4}, \quad B_1 = 0, \quad B_{-1} = \frac{1}{16}.$$

Similarly, we get:

$$U_{21}(x,y,t) = \frac{1}{16}\left(\frac{2}{\sqrt{\lambda^2-4\mu}}\coth\left(\frac{\sqrt{\lambda^2-4\mu}}{2}(x+y-\omega t)\right)\right) + \frac{1}{4}. \tag{3.14}$$

$$U_{22}(x,y,t) = \frac{1}{16}\left(\frac{2}{\sqrt{\lambda^2-4\mu}}\tanh\left(\frac{\sqrt{\lambda^2-4\mu}}{2}(x+y-\omega t)\right)\right) + \frac{1}{4}. \tag{3.15}$$

$$U_{23}(x,y,t) = \frac{1}{16}(x+y-\omega t) + \frac{1}{4}. \tag{3.16}$$

$$U_{24}(x,y,t) = \frac{i}{16}\left(\frac{2}{\sqrt{\lambda^2-4\mu}}\cot\left(i\frac{\sqrt{\lambda^2-4\mu}}{2}(x+y-\omega t)\right)\right) + \frac{1}{4}. \tag{3.17}$$

$$U_{25}(x,y,t) = -\frac{i}{16}\left(\frac{2}{\sqrt{\lambda^2-4\mu}}\tan\left(i\frac{\sqrt{\lambda^2-4\mu}}{2}(x+y-\omega t)\right)\right) + \frac{1}{4} \tag{3.18}$$

**Case III:**

$$\lambda = \lambda, \quad \mu = \frac{\lambda^2}{4} - \frac{1}{16}, \quad \omega = -\frac{1}{4}, \quad B_0 = \frac{1}{4}, \quad B_1 = 1, \quad B_{-1} = 0.$$

In the same manner, we obtain:

$$U_{31}(x,y,t) = \frac{\sqrt{\lambda^2-4\mu}}{2}\tanh\left(\frac{\sqrt{\lambda^2-4\mu}}{2}(x+y-\omega t)\right) + \frac{1}{4}. \tag{3.19}$$

$$U_{32}(x,y,t) = \frac{\sqrt{\lambda^2-4\mu}}{2}\coth\left(\frac{\sqrt{\lambda^2-4\mu}}{2}(x+y-\omega t)\right) + \frac{1}{4}. \tag{3.20}$$

$$U_{33}(x,y,t) = \frac{1}{x+y-\omega t} + \frac{1}{4} \tag{3.21}$$

$$U_{34}(x,y,t) = -\frac{\sqrt{-(\lambda^2-4\mu)}}{2}\tan\left(\frac{\sqrt{-(\lambda^2-4\mu)}}{2}(x+y-\omega t)\right) + \frac{1}{4} \tag{3.22}$$

$$U_{35}(x,y,t) = \frac{\sqrt{-(\lambda^2-4\mu)}}{2}\cot\left(\frac{\sqrt{-(\lambda^2-4\mu)}}{2}(x+y-\omega t)\right) + \frac{1}{4} \tag{3.23}$$

**Case IV:**

$$\lambda = \lambda, \quad \mu = \frac{\lambda^2}{4} - \frac{1}{16}, \quad \omega = -\frac{1}{4}, \quad B_0 = \frac{1}{4}, \quad B_1 = -1, \quad B_{-1} = 0.$$

Likewise, it follows that:

$$U_{41}(x,y,t) = -\frac{\sqrt{\lambda^2-4\mu}}{2}\tanh\left(\frac{\sqrt{\lambda^2-4\mu}}{2}(x+y-\omega t)\right) + \frac{1}{4}. \tag{3.24}$$

$$U_{42}(x,y,t) = -\frac{\sqrt{\lambda^2-4\mu}}{2}\coth\left(\frac{\sqrt{\lambda^2-4\mu}}{2}(x+y-\omega t)\right)+\frac{1}{4}. \tag{3.25}$$

$$U_{43}(x,y,t) = -\frac{1}{x+y-\omega t}+\frac{1}{4}. \tag{3.26}$$

$$U_{44}(x,y,t) = -\left(-\frac{\sqrt{-(\lambda^2-4\mu)}}{2}\tan\left(\frac{\sqrt{-(\lambda^2-4\mu)}}{2}(x+y-\omega t)\right)\right)+\frac{1}{4}. \tag{3.27}$$

$$U_{45}(x,y,t) = -\frac{\sqrt{-(\lambda^2-4\mu)}}{2}\cot\left(\frac{\sqrt{-(\lambda^2-4\mu)}}{2}(x+y-\omega t)\right)+\frac{1}{4}. \tag{3.28}$$

**Case V:**

$$\lambda=\lambda,\quad \mu=\frac{\lambda^2}{4}+\frac{1}{32},\quad \omega=-\frac{1}{4},\quad B_0=\frac{1}{4},\quad B_1=1,\quad B_{-1}=\frac{1}{32}.$$

Analogously, we derive:

$$\begin{aligned}U_{51}(x,y,t) = {}& \frac{1}{32}\left(\frac{2}{\sqrt{\lambda^2-4\mu}}\coth\left(\frac{\sqrt{\lambda^2-4\mu}}{2}(x+y-\omega t)\right)\right)\\ &+\frac{\sqrt{\lambda^2-4\mu}}{2}\tanh\left(\frac{\sqrt{\lambda^2-4\mu}}{2}(x+y-\omega t)\right)+\frac{1}{4},\end{aligned} \tag{3.29}$$

$$\begin{aligned}U_{52}(x,y,t) = {}& \frac{1}{32}\left(\frac{2}{\sqrt{\lambda^2-4\mu}}\tanh\left(\frac{\sqrt{\lambda^2-4\mu}}{2}(x+y-\omega t)\right)\right)\\ &+\frac{\sqrt{\lambda^2-4\mu}}{2}\coth\left(\frac{\sqrt{\lambda^2-4\mu}}{2}(x+y-\omega t)\right)+\frac{1}{4},\end{aligned} \tag{3.30}$$

$$U_{53}(x,y,t) = \frac{1}{32}(x+y-\omega t)+\frac{1}{x+y-\omega t}+\frac{1}{4}, \tag{3.31}$$

$$\begin{aligned}U_{54}(x,y,t) = {}& \frac{i}{32}\left(\frac{2}{\sqrt{\lambda^2-4\mu}}\cot\left(i\frac{\sqrt{\lambda^2-4\mu}}{2}(x+y-\omega t)\right)\right)\\ &-\frac{\sqrt{-(\lambda^2-4\mu)}}{2}\tan\left(\frac{\sqrt{-(\lambda^2-4\mu)}}{2}(x+y-\omega t)\right)+\frac{1}{4},\end{aligned} \tag{3.32}$$

$$\begin{aligned}U_{55}(x,y,t) = {}& -\frac{i}{32}\left(\frac{2}{\sqrt{\lambda^2-4\mu}}\tan\left(i\frac{\sqrt{\lambda^2-4\mu}}{2}(x+y-\omega t)\right)\right)\\ &+\frac{\sqrt{-(\lambda^2-4\mu)}}{2}\cot\left(\frac{\sqrt{-(\lambda^2-4\mu)}}{2}(x+y-\omega t)\right)+\frac{1}{4}.\end{aligned} \tag{3.33}$$

**Case VI:**

$$\lambda=\lambda,\quad \mu=\frac{\lambda^2}{4}-\frac{1}{64},\quad \omega=-\frac{1}{4},\quad B_0=\frac{1}{4},\quad B_1=1,\quad B_{-1}=\frac{1}{64}.$$

Following the same approach, we find:

$$U_{61}(x,y,t) = \frac{1}{64}\left(\frac{2}{\sqrt{\lambda^2-4\mu}}\coth\left(\frac{\sqrt{\lambda^2-4\mu}}{2}(x+y-\omega t)\right)\right) + \frac{\sqrt{\lambda^2-4\mu}}{2}\tanh\left(\frac{\sqrt{\lambda^2-4\mu}}{2}(x+y-\omega t)\right)+\frac{1}{4}. \tag{3.34}$$

$$U_{62}(x,y,t) = \frac{1}{64}\left(\frac{2}{\sqrt{\lambda^2-4\mu}}\tanh\left(\frac{\sqrt{\lambda^2-4\mu}}{2}(x+y-\omega t)\right)\right) + \frac{\sqrt{\lambda^2-4\mu}}{2}\coth\left(\frac{\sqrt{\lambda^2-4\mu}}{2}(x+y-\omega t)\right)+\frac{1}{4}. \tag{3.35}$$

$$U_{63}(x,y,t) = \frac{1}{64}(x+y-\omega t)+\frac{1}{x+y-\omega t}+\frac{1}{4}. \tag{3.36}$$

$$U_{64}(x,y,t) = \frac{i}{64}\left(\frac{2}{\sqrt{\lambda^2-4\mu}}\cot\left(i\frac{\sqrt{\lambda^2-4\mu}}{2}(x+y-\omega t)\right)\right) - \frac{\sqrt{-(\lambda^2-4\mu)}}{2}\tan\left(\frac{\sqrt{-(\lambda^2-4\mu)}}{2}(x+y-\omega t)\right)+\frac{1}{4}. \tag{3.37}$$

$$U_{65}(x,y,t) = -\frac{i}{64}\left(\frac{2}{\sqrt{\lambda^2-4\mu}}\tan\left(i\frac{\sqrt{\lambda^2-4\mu}}{2}(x+y-\omega t)\right)\right) + \frac{\sqrt{-(\lambda^2-4\mu)}}{2}\cot\left(\frac{\sqrt{-(\lambda^2-4\mu)}}{2}(x+y-\omega t)\right)+\frac{1}{4}. \tag{3.38}$$

**Case VII:**

$$\lambda=\lambda,\quad \mu=\frac{\lambda^2}{4}-\frac{1}{64},\quad \omega=-\frac{1}{4},\quad B_0=\frac{1}{4},\quad B_1=-1,\quad B_{-1}=-\frac{1}{64}.$$

Using a similar method, we have:

$$U_{71}(x,y,t) = -\frac{1}{64}\left(\frac{2}{\sqrt{\lambda^2-4\mu}}\coth\left(\frac{\sqrt{\lambda^2-4\mu}}{2}(x+y-\omega t)\right)\right) - \frac{\sqrt{\lambda^2-4\mu}}{2}\tanh\left(\frac{\sqrt{\lambda^2-4\mu}}{2}(x+y-\omega t)\right)+\frac{1}{4}. \tag{3.39}$$

$$U_{72}(x,y,t) = -\frac{1}{64}\left(\frac{2}{\sqrt{\lambda^2-4\mu}}\tanh\left(\frac{\sqrt{\lambda^2-4\mu}}{2}(x+y-\omega t)\right)\right) - \frac{\sqrt{\lambda^2-4\mu}}{2}\coth\left(\frac{\sqrt{\lambda^2-4\mu}}{2}(x+y-\omega t)\right)+\frac{1}{4}. \tag{3.40}$$

$$U_{73}(x,y,t) = -\frac{1}{64}(x+y-\omega t)-\frac{1}{x+y-\omega t}+\frac{1}{4} \tag{3.41}$$

$$U_{74}(x,y,t) = -\frac{i}{64}\left(\frac{2}{\sqrt{\lambda^2-4\mu}}\cot\left(i\frac{\sqrt{\lambda^2-4\mu}}{2}(x+y-\omega t)\right)\right) + \frac{\sqrt{-(\lambda^2-4\mu)}}{2}\tan\left(\frac{\sqrt{-(\lambda^2-4\mu)}}{2}(x+y-\omega t)\right)+\frac{1}{4} \tag{3.42}$$

$$U_{75}(x,y,t) = \frac{i}{64}\left(\frac{2}{\sqrt{\lambda^2-4\mu}}\tan\left(i\frac{\sqrt{\lambda^2-4\mu}}{2}(x+y-\omega t)\right)\right) - \frac{\sqrt{-(\lambda^2-4\mu)}}{2}\cot\left(\frac{\sqrt{-(\lambda^2-4\mu)}}{2}(x+y-\omega t)\right)+\frac{1}{4}. \tag{3.43}$$

**Case VIII:**

$$\lambda=\lambda,\quad \mu=\frac{\lambda^2}{4}+\frac{1}{32},\quad \omega=-\frac{1}{4},\quad B_0=\frac{1}{4},\quad B_1=-1,\quad B_{-1}=-\frac{1}{32}.$$

By a comparable argument, we get:

$$U_{81}(x,y,t) = -\frac{1}{32}\left(\frac{2}{\sqrt{\lambda^2-4\mu}}\coth\left(\frac{\sqrt{\lambda^2-4\mu}}{2}(x+y-\omega t)\right)\right) - \frac{\sqrt{\lambda^2-4\mu}}{2}\tanh\left(\frac{\sqrt{\lambda^2-4\mu}}{2}(x+y-\omega t)\right)+\frac{1}{4}. \tag{3.44}$$

$$U_{82}(x,y,t) = -\frac{1}{32}\left(\frac{2}{\sqrt{\lambda^2-4\mu}}\tanh\left(\frac{\sqrt{\lambda^2-4\mu}}{2}(x+y-\omega t)\right)\right) - \frac{\sqrt{\lambda^2-4\mu}}{2}\coth\left(\frac{\sqrt{\lambda^2-4\mu}}{2}(x+y-\omega t)\right)+\frac{1}{4}. \tag{3.45}$$

$$U_{83}(x,y,t) = -\frac{1}{32}(x+y-\omega t)-\frac{1}{x+y-\omega t}+\frac{1}{4}. \tag{3.46}$$

$$U_{84}(x,y,t) = -\frac{i}{32}\left(\frac{2}{\sqrt{\lambda^2-4\mu}}\cot\left(i\frac{\sqrt{\lambda^2-4\mu}}{2}(x+y-\omega t)\right)\right) + \frac{\sqrt{-(\lambda^2-4\mu)}}{2}\tan\left(\frac{\sqrt{-(\lambda^2-4\mu)}}{2}(x+y-\omega t)\right)+\frac{1}{4}. \tag{3.47}$$

$$U_{85}(x,y,t) = \frac{i}{32}\left(\frac{2}{\sqrt{\lambda^2-4\mu}}\tan\left(i\frac{\sqrt{\lambda^2-4\mu}}{2}(x+y-\omega t)\right)\right) - \frac{\sqrt{-(\lambda^2-4\mu)}}{2}\cot\left(\frac{\sqrt{-(\lambda^2-4\mu)}}{2}(x+y-\omega t)\right)+\frac{1}{4}. \tag{3.48}$$

## 4. Results and discussion

Let us explore a comparative analysis of the exact soliton solutions (ESSs) derived using the $mG'/GE$ process method and the EMRE method [15], focusing on their application to the JMH equation. Both methods are unique approaches within mathematical physics, each offering distinct features and advantages. In the research by Iqbal et al. [15], the JMH equation was investigated using the EMRE method, resulting in the identification of thirty solutions. In contrast, our study employed the $mG'/GE$ process, leading to the discovery of forty distinct ESSs expressed through hyperbolic, trigonometric, and exponential functions. The solutions we derived in our analysis differ significantly from those obtained by Iqbal et al. [15]. A key distinction lies in the auxiliary equation utilized in our method, which enabled us to uncover new types of solutions that were not accessible through methods like the EMRE approach. This highlights the versatility and effectiveness of the $mG'/GE$ process in generating novel and diverse solutions for the JMH equation.

In this section, we delve into comprehensive discussions comparing the solutions that we have derived. Additionally, we present graphical representations characterized by various free parameters and showcasing the following aspects of our obtained solutions of JMH equation by applying $mG'/GE$ process. Various types of 3D, contour and 2D plots illustrating the derived solutions are generated using MATLAB software, allowing for a comprehensive analysis of their nature. To emphasize this point, by assigning different values to the free parameters we have generated plots depicting the solutions of the Equations (3.9), (3.10), (3.14), (3.15), (3.32), (3.33), (3.47) and (3.48). This explorations showcases different types of exact soliton solutions including kink solitons, bright and dark solitons, periodic traveling waves, and their combinations. The combinations of different types of parameters utilized in the study may result in the emergence of diverse soliton solutions. The solution (3.9) describes a solution with dark soliton, where parameters $\lambda = 0.1$, $\mu = -0.06$ , $\omega = -0.25$ , $t = 0.001$ are employed. This solution is illustrated in Fig. **??**(1a–1c): 3D, contour, and 2D (at different time levels) plots, respectively, for the limits $-10 \leq x \leq 10$, $-10 \leq y \leq 10$. Next, Figure 1(1d–1f) illustrates a singular kink soliton as 3D, contour, and 2D (at different time levels) plots, respectively, for the limits $-10 \leq x \leq 10$, $-10 \leq y \leq 10$, using parameters $\lambda = 0.1$, $\mu = -0.06$, $\omega = -0.25$, and $t = 1$. Then, Figure 1(1g–1i) illustrates 3D, contour, and 2D (at different time levels) plots, respectively, for the limits $-10 \leq x \leq 10$, $-10 \leq y \leq 10$, using parameters $\lambda = 0.01$, $\mu = -0.0625$, $\omega = -0.25$, and $t = 10$. And Figure 1(1j–1l) illustrates 3D, contour, and 2D (at different time levels) plots, respectively, for the limits $-10 \leq x \leq 10$, $-10 \leq y \leq 10$, using parameters $\lambda = 0.1$, $\mu = -0.06$, $\omega = -0.25$, and $t = 100$. The expression (3.10) represents a solution with an anti-kink shape, observed for the parameters $\lambda = 0.1$, $\mu = -0.06$, $\omega = -0.25$, and $t = 0.01$. This solution is illustrated in Figure **??**(2a–2c): 3D, contour, and 2D (at different time levels) plots, respectively, for the limits $-10 \leq x \leq 10$, $-10 \leq y \leq 10$. Next, Figure 2(2d–2f) illustrates 3D, contour, and 2D (at different time levels) plots, respectively, for the limits $-10 \leq x \leq 10$, $-10 \leq y \leq 10$, using parameters $\lambda = 0.01$, $\mu = -0.0625$, $\omega = -0.25$, and $t = 1$. Then, Figure 2(2g–2i) illustrates 3D, contour, and 2D (at different time levels) plots, respectively, for the limits $-10 \leq x \leq 10$, $-10 \leq y \leq 10$, using parameters $\lambda = 0.1$, $\mu = -0.06$, $\omega = -0.25$, and $t = 10$. And Figure 2(2j–2l) illustrates 3D, contour, and 2D (at different time levels) plots, respectively, for the limits $-10 \leq x \leq 10$, $-10 \leq y \leq 10$, using parameters $\lambda = -0.01$, $\mu = -0.0625$, $\omega = -0.25$, and $t = 100$. The solution (3.14) describes the feature of the bright soliton, where the parameters used are $\lambda = 0.1$, $\mu = -0.06$, $\omega = -0.25$, and $t = 0.01$. This solution is illustrated in Figure 3(3a–3c) by the 3D, contour, and 2D (at different time levels) plots, respectively, for the domain $-10 \leq x \leq 10$, $-10 \leq y \leq 10$. Next, Figure 3(3d–3f) illustrates the 3D, contour, and 2D (at different time levels) plots, respectively, for the domain $-10 \leq x \leq 10$, $-10 \leq y \leq 10$, using the parameters $\lambda = 0.01$, $\mu = -0.0625$, $\omega = -0.25$, and $t = 1$. Then, Figure 3(3g–3i) illustrates the 3D, contour, and 2D (at different time levels) plots, respectively, for the domain $-10 \leq x \leq 10$, $-10 \leq y \leq 10$, using the parameters $\lambda = 0.1$, $\mu = -0.06$, $\omega = -0.25$, and $t = 10$. And Figure 3(3j–3l) illustrates the 3D, contour, and 2D (at different time levels) plots, respectively, for the domain $-10 \leq x \leq 10$, $-10 \leq y \leq 10$, using the parameters $\lambda = -0.1$, $\mu = -0.06$, $\omega = -0.25$, and $t = 100$. The anti-kink soliton, depicted in Figure 4, is represented by the solution (3.15), where the parameters $\lambda = 0.1$, $\mu = -0.06$, $\omega = -0.25$, and $t = 0.01$ are employed. This solution is illustrated in Figure 4(4a–4c) by the 3D, contour, and 2D (at different time levels) plots, respectively, for the domain $-10 \leq x \leq 10$, $-10 \leq y \leq 10$. Next, Figure 4(4d–4f) represents the 3D, contour, and 2D (at different time levels) plots, respectively, for the same domain, using the parameters $\lambda = 0.1$, $\mu = -0.06$, $\omega = -0.25$, and $t = 1$. Then, Figure 4(4g–4i) illustrates the 3D, contour, and 2D (at different time levels) plots, respectively, for the domain

$-10 \leq x \leq 10$, $-10 \leq y \leq 10$, using the parameters $\lambda = 0.01$, $\mu = -0.0625$, $\omega = -0.25$, and $t = 20$. Furthermore, Figure 4(4j–4l) presents the 3D, contour, and 2D (at different time levels) plots, respectively, for the same domain, using the parameters $\lambda = 0.01$, $\mu = -0.0625$, $\omega = -0.25$, and $t = 150$. The anti-kink soliton, as depicted in Figure 5, is represented by the solution (3.32), where the parameters $\lambda = 0.01$, $\mu = 0.0313$, $\omega = -0.25$, and $t = 0.01$ are employed. This solution is illustrated in Figure 5(5a–5c) by the 3D, contour, and 2D (at different time levels) plots, respectively, for the domain $-10 \leq x \leq 10$, $-10 \leq y \leq 10$. Next, Figure 5(5d–5f) showcases the 3D, contour, and 2D (at different time levels) plots, respectively, for the domain $-10 \leq x \leq 10$, $-10 \leq y \leq 10$, using the parameters $\lambda = 0.1$, $\mu = 0.0338$, $\omega = -0.25$, and $t = 1$. Then, Figure 5(5g–5i) shows the 3D, contour, and 2D (at different time levels) plots, respectively, for the domain $-10 \leq x \leq 10$, $-10 \leq y \leq 10$, using the parameters $\lambda = 0.01$, $\mu = 0.0313$, $\omega = -0.25$, and $t = 15$. And Figure 5(5j–5l) illustrates the 3D, contour, and 2D (at different time levels) plots, respectively, for the domain $-10 \leq x \leq 10$, $-10 \leq y \leq 10$, using the parameters $\lambda = 0.01$, $\mu = 0.0313$, $\omega = -0.25$, and $t = 150$. The anti-kink soliton represented in Figure 6 is expressed by the solution (3.33), where the parameters $\lambda = 0.01$, $\mu = 0.0313$, $\omega = -0.25$, and $t = 0.01$ are employed. This solution is illustrated in Figure 6(6a–6c) by the 3D, contour, and 2D (at different time levels) plots, respectively, for the domain $-10 \leq x \leq 10$, $-10 \leq y \leq 10$. Next, Fig 6(6d–6f) explores the 3D, contour, and 2D (at different time levels) plots, respectively, for the same domain, using the parameters $\lambda = 0.1$, $\mu = 0.0338$, $\omega = -0.25$, and $t = 1$. Then, Figure 6(6g–6i) illustrates the 3D, contour, and 2D (at different time levels) plots, respectively, for the domain $-10 \leq x \leq 10$, $-10 \leq y \leq 10$, using the parameters $\lambda = 0.1$, $\mu = 0.0338$, $\omega = -0.25$, and $t = 15$. Finally, Figure 6(6j–6l) manifests the 3D, contour, and 2D (at different time levels) plots, respectively, for the domain $-10 \leq x \leq 10$, $-10 \leq y \leq 10$, using the parameters $\lambda = 0.01$, $\mu = 0.0313$, $\omega = -0.25$, and $t = 150$. The anti-kink soliton, depicted in Figure 7, is expressed by the solution (3.47), where the parameters $\lambda = 0.01$, $\mu = 0.0313$, $\omega = -0.25$, and $t = 0.01$ are employed. This solution is illustrated in Figure 7(7a–7c) by the 3D, contour, and 2D (at different time levels) plots, respectively, for the domain $-10 \leq x \leq 10$, $-10 \leq y \leq 10$. Next, Figure 7(7d–7f) is plotted as the 3D, contour, and 2D (at different time levels) plots, respectively, for the same domain, using the parameters $\lambda = 0.5$, $\mu = 0.0938$, $\omega = -0.25$, and $t = 0.1$. Then, Figure 7(7g–7i) illustrates the 3D, contour, and 2D (at different time levels) plots, respectively, for the domain $-10 \leq x \leq 10$, $-10 \leq y \leq 10$, using the parameters $\lambda = 0.05$, $\mu = 0.0319$, $\omega = -0.25$, and $t = 10$. Finally, Figure 7(7j–7l) expresses the 3D, contour, and 2D (at different time levels) plots, respectively, for the domain $-10 \leq x \leq 10$, $-10 \leq y \leq 10$, using the parameters $\lambda = 0.5$, $\mu = 0.0938$, $\omega = -0.25$, and $t = 100$. The anti-kink soliton, manifested in Figure 8, is expressed by the solution (3.48), where the parameters $\lambda = 0.05$, $\mu = -0.06$, $\omega = -0.25$, and $t = 0.001$ are employed. This solution is illustrated in Figure 8(8a–8c) by the 3D, contour, and 2D (at different time levels) plots, respectively, for the domain $-10 \leq x \leq 10$, $-10 \leq y \leq 10$. Figure 8(8d–8f) illustrates the 3D, contour, and 2D (at different time levels) plots, respectively, for the same domain, using the parameters $\lambda = 0.5$, $\mu = -0.06$, $\omega = -0.25$, and $t = 0.1$. Figure 8(8g–8i) illustrates the 3D, contour, and 2D (at different time levels) plots, respectively, for the domain $-10 \leq x \leq 10$, $-10 \leq y \leq 10$, using the parameters $\lambda = 0.05$, $\mu = -0.06$, $\omega = -0.25$, and $t = 10$. Finally, Figure 8(8j–8l) illustrates the 3D, contour, and 2D (at different time levels) plots, respectively, for the domain $-10 \leq x \leq 10$, $-10 \leq y \leq 10$, using the parameters $\lambda = 0.05$, $\mu = -0.06$, $\omega = -0.25$, and $t = 100$.



## 5. Conclusion

In this study, we have effectively applied $mG'/GE$ process to demonstrate its practical and efficient approach in solving the JMH equation. We have successfully derived forty novel exact soliton solutions that capture a diverse range of solitary wave phenomena. These include dark solitons, kink solitons, bright solitons, anti-kink solitons and periodic solitons solutions. The JM hierarchy equation's exact soliton solutions have significant physical implications. These soliton solutions approximate the consistent structures found in genuine physical systems, such as optical fibres or shallow water channels, where their presence is necessary for maintaining wave integrity over long distances. Our findings establish a deeper physical understanding of nonlinear wave propagation by demonstrating how changes in model parameters affect soliton behaviour. Future studies might expand these findings for experimental validations or engineering system applications. Detailed graphical representations, including 3D, 2D, and contour plots, illustrate the intricate behavior of these new soliton solutions. These visualizations highlight how various parameters influence their traveling behavior, offering deeper understandings into the dynamics of the solutions. The $mG'/GE$ process

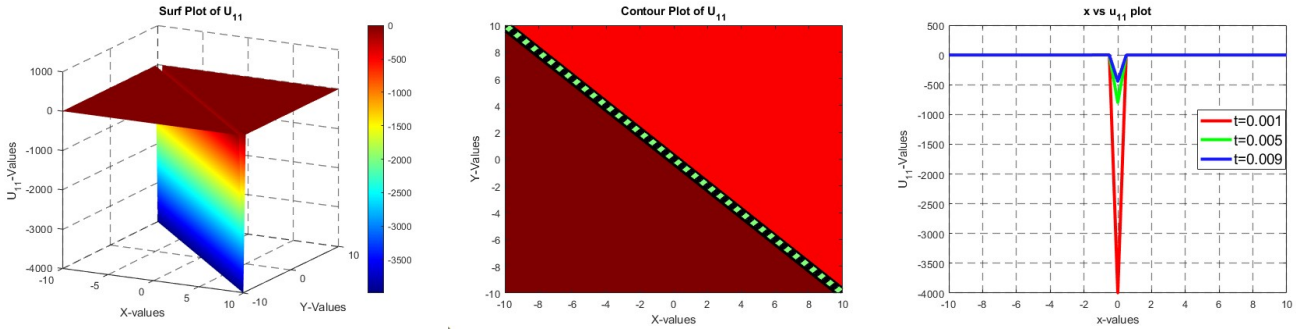


(a) 3D plot (b) Contour plot (c) 2D plot

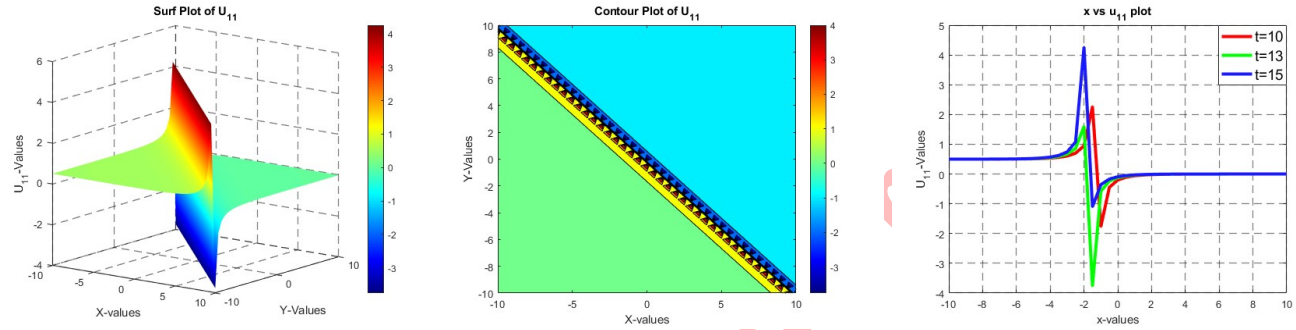


(d) 3D plot (e) Contour plot (f) 2D plot

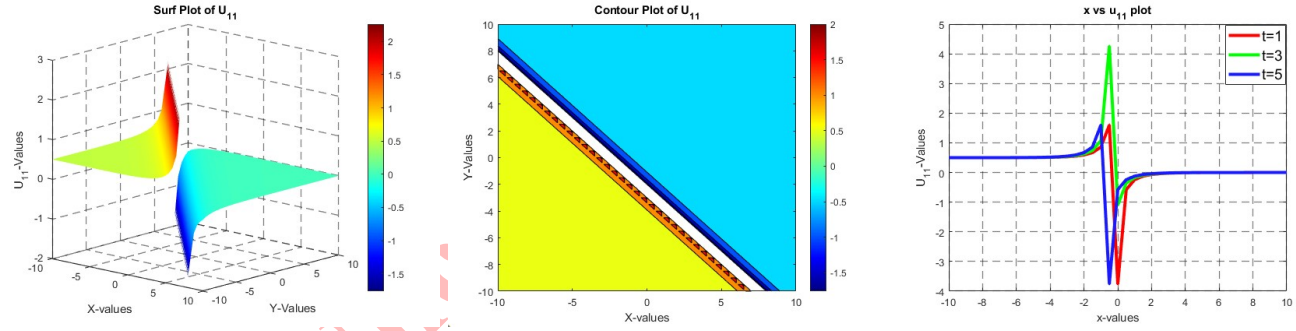


(g) 3D plot (h) Contour plot (i) 2D plot

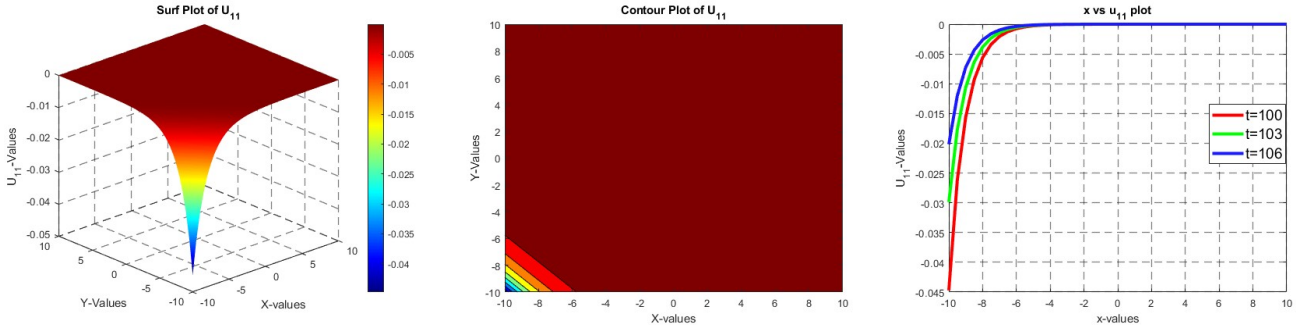


(j) 3D plot (k) Contour plot (l) 2D plot

**Figure 1.** Shapes for the equation (3.9).

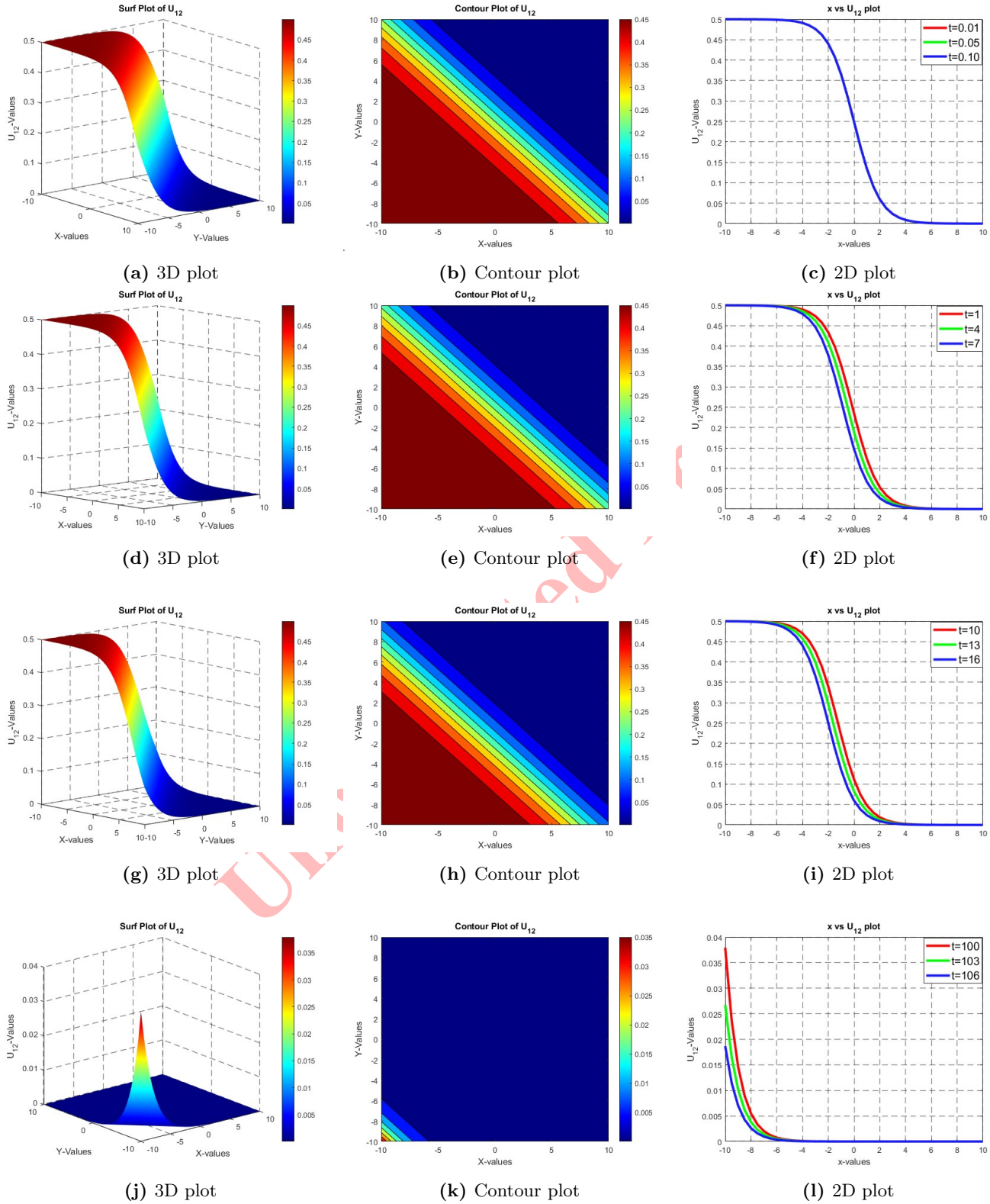


**(a)** 3D plot **(b)** Contour plot **(c)** 2D plot

**(d)** 3D plot **(e)** Contour plot **(f)** 2D plot

**(g)** 3D plot **(h)** Contour plot **(i)** 2D plot

**(j)** 3D plot **(k)** Contour plot **(l)** 2D plot

**Figure 2.** Shapes for the Equation (3.10).

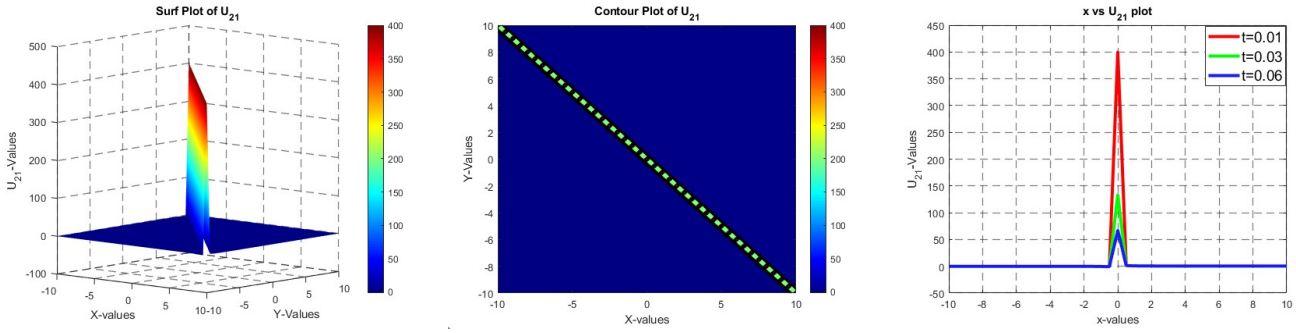


**(a)** 3D plot **(b)** Contour plot **(c)** 2D plot

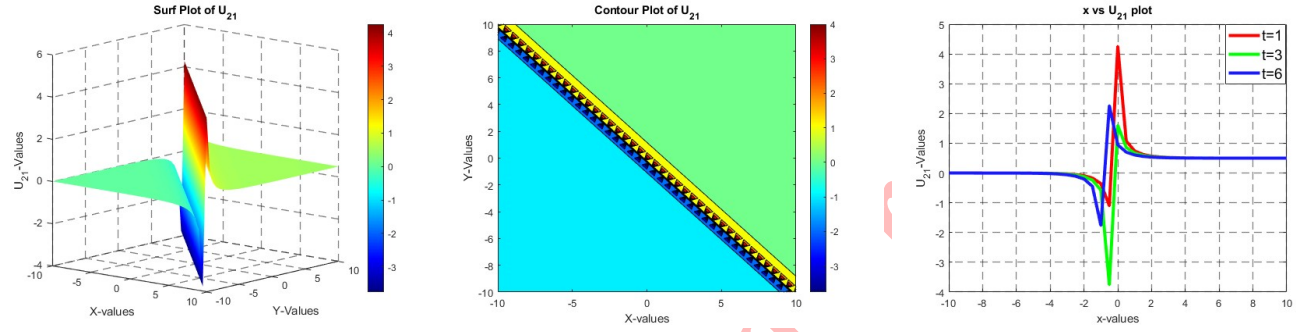


**(d)** 3D plot **(e)** Contour plot **(f)** 2D plot

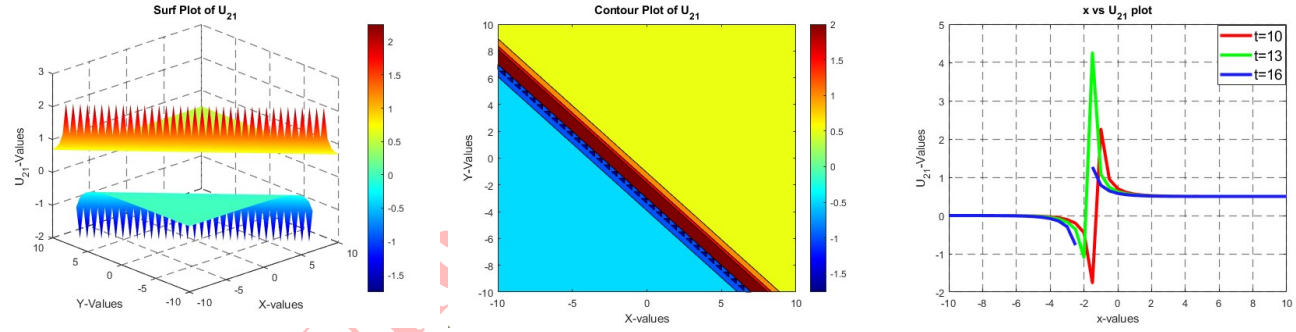


**(g)** 3D plot **(h)** Contour plot **(i)** 2D plot

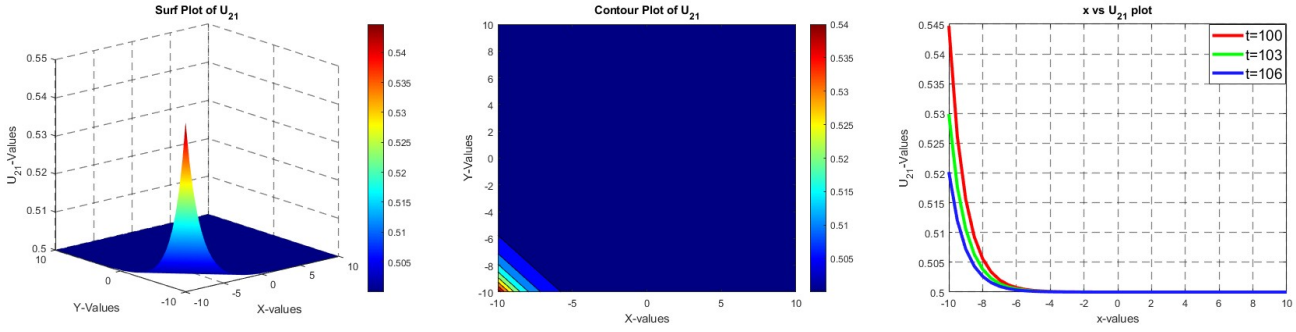


**(j)** 3D plot **(k)** Contour plot **(l)** 2D plot

**Figure 3.** Shapes for the Equation (3.14).

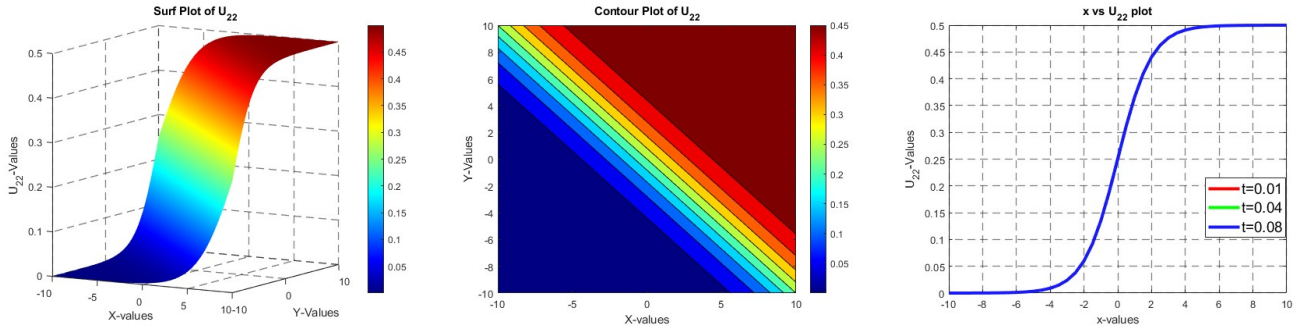


**(a)** 3D plot **(b)** Contour plot **(c)** 2D plot

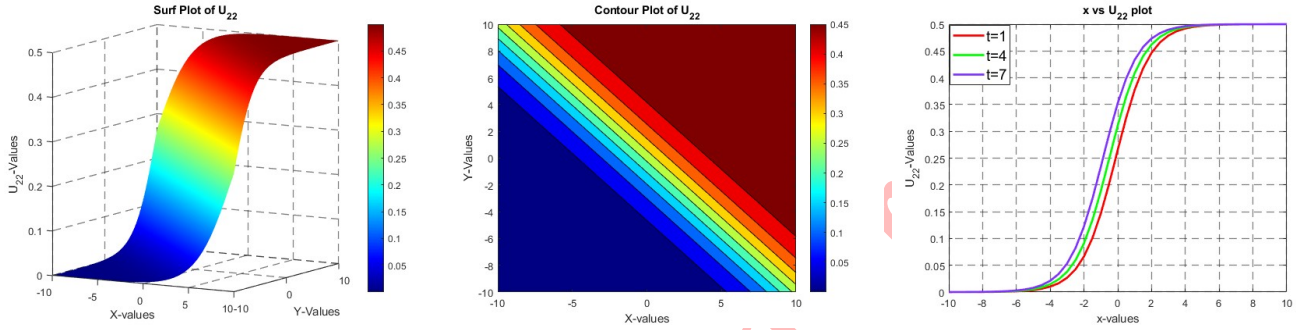


**(d)** 3D plot **(e)** Contour plot **(f)** 2D plot

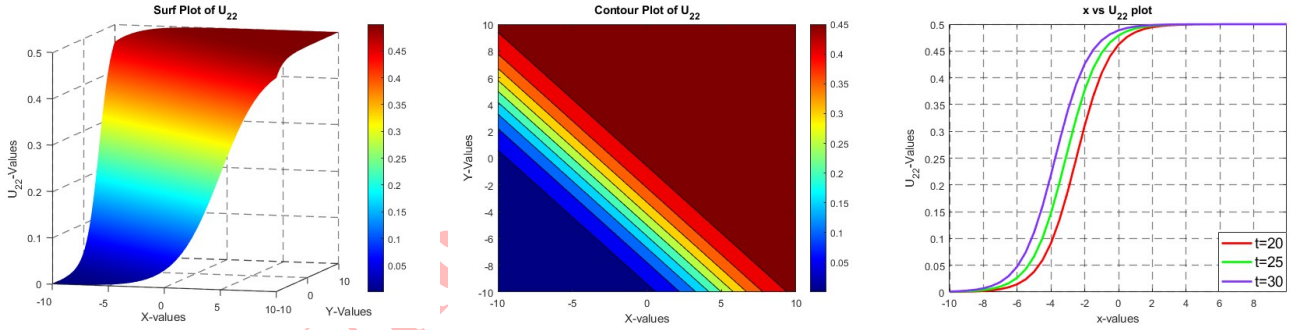


**(g)** 3D plot **(h)** Contour plot **(i)** 2D plot

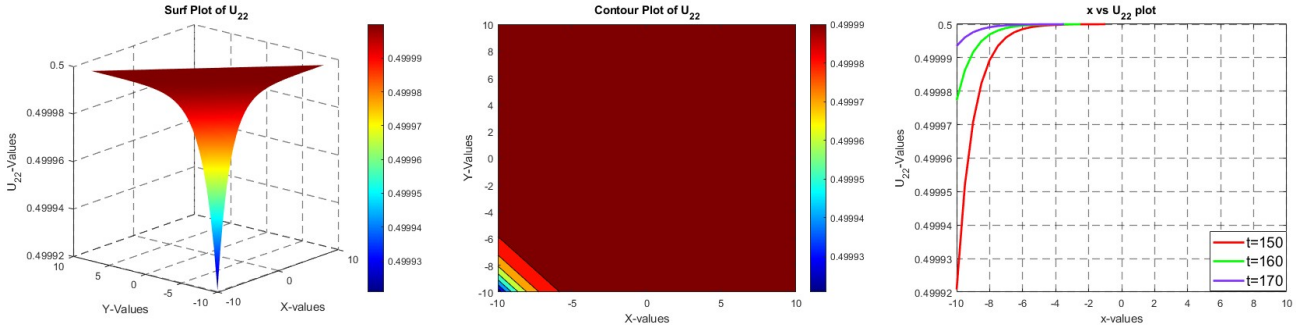


**(j)** 3D plot **(k)** Contour plot **(l)** 2D plot

**Figure 4.** Shapes for the Equation (3.15).

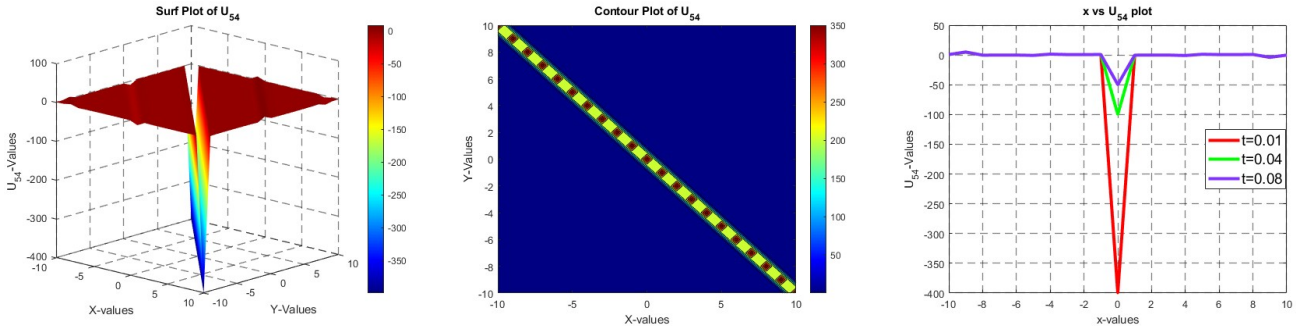


(a) 3D plot (b) Contour plot (c) 2D plot

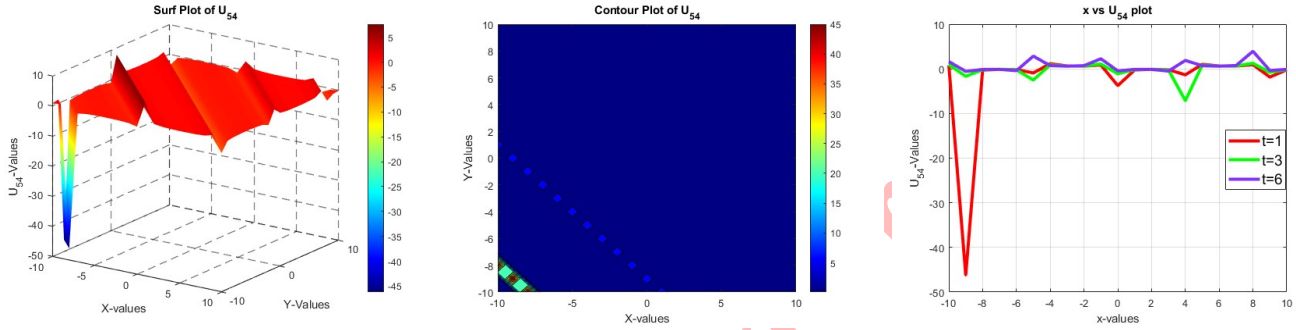


(d) 3D plot (e) Contour plot (f) 2D plot

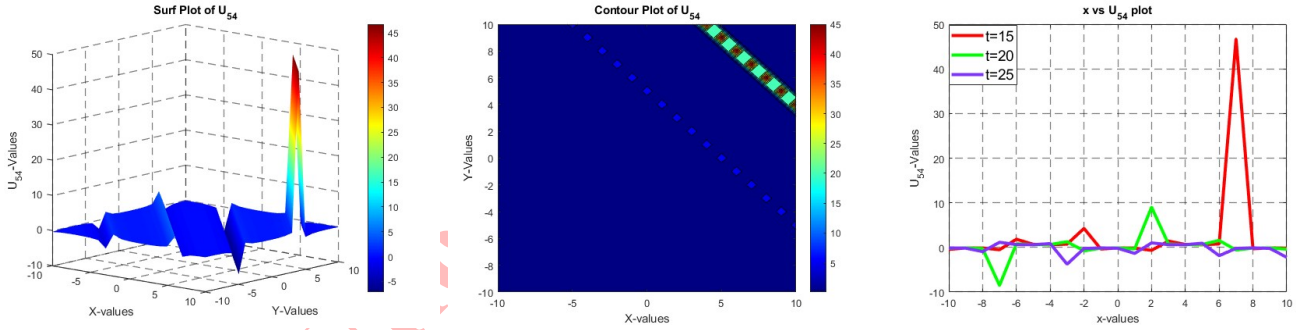


(g) 3D plot (h) Contour plot (i) 2D plot

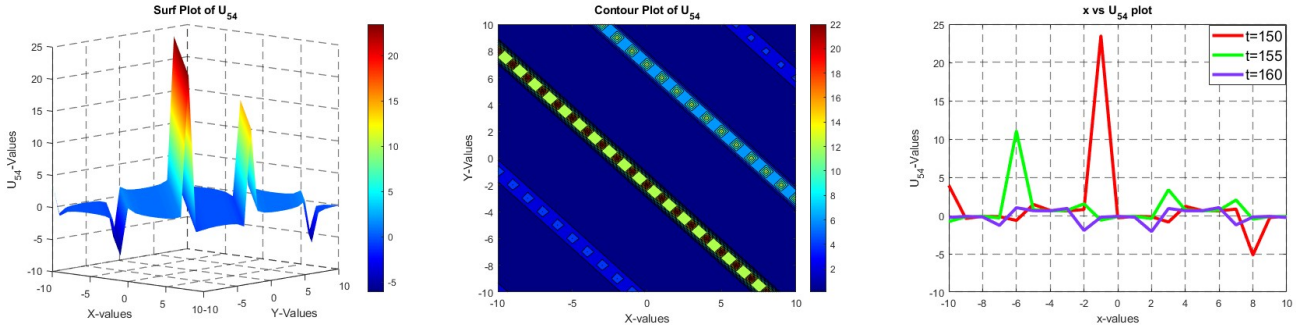


(j) 3D plot (k) Contour plot (l) 2D plot

**Figure 5.** Shapes for the Equation (3.32).

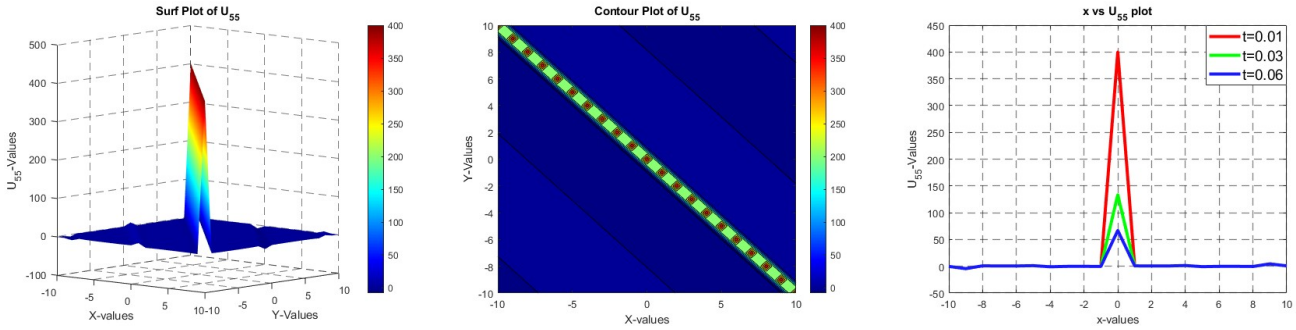


**(a)** 3D plot **(b)** Contour plot **(c)** 2D plot

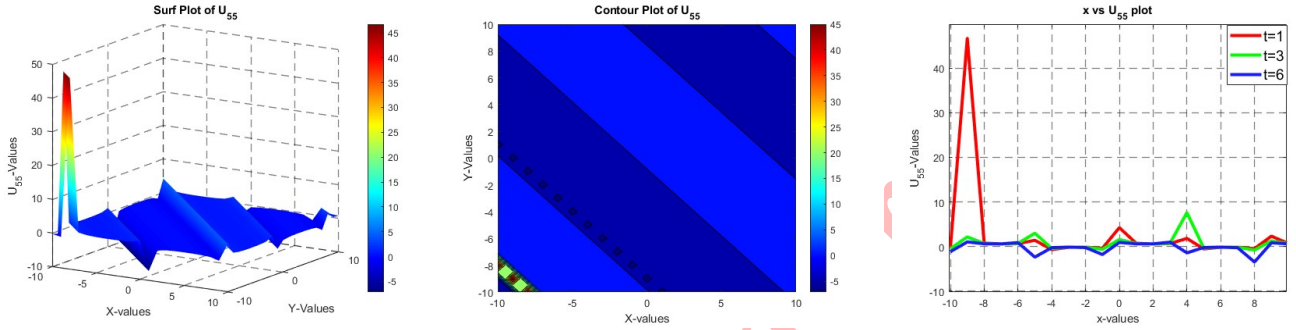


**(d)** 3D plot **(e)** Contour plot **(f)** 2D plot

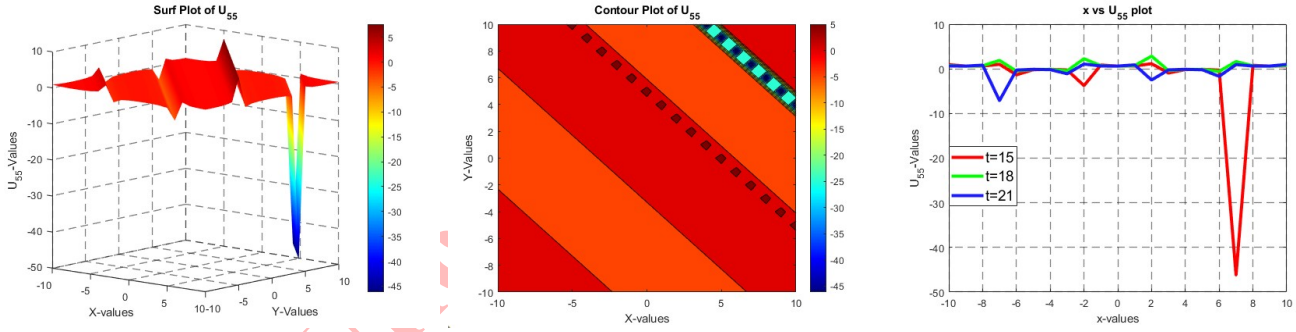


**(g)** 3D plot **(h)** Contour plot **(i)** 2D plot

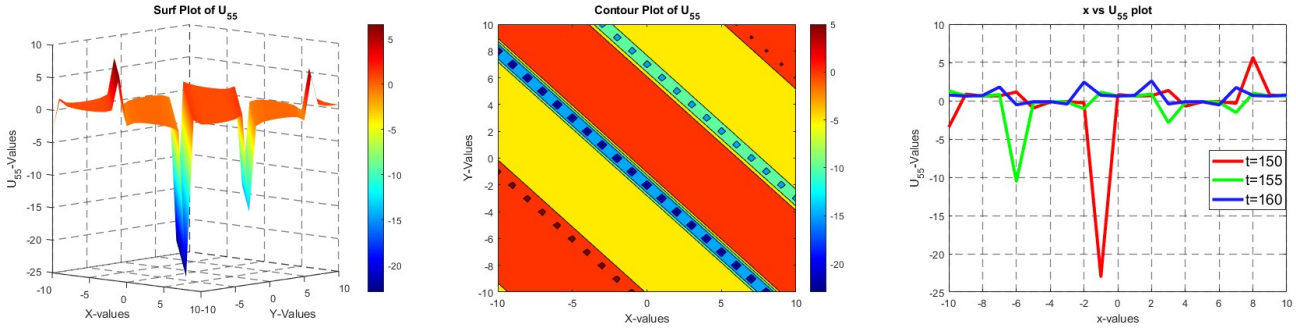


**(j)** 3D plot **(k)** Contour plot **(l)** 2D plot

**Figure 6.** Shapes for the Equation (3.33).

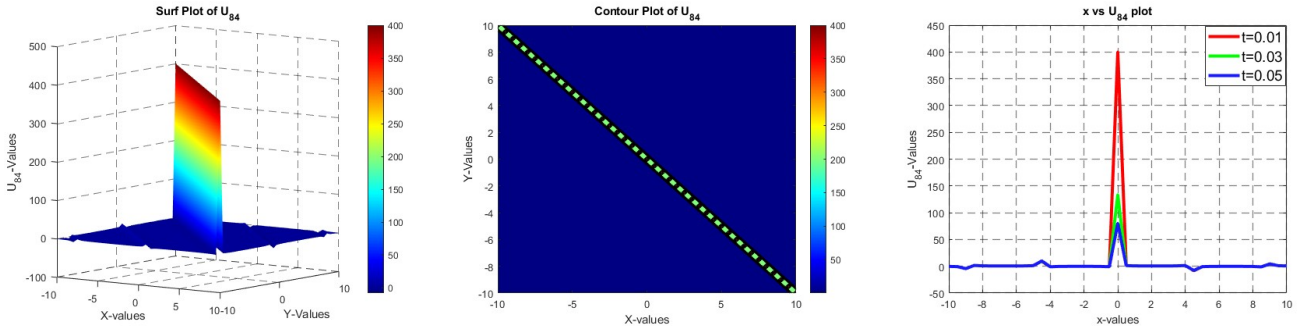


(a) 3D plot




(b) Contour plot




(c) 2D plot

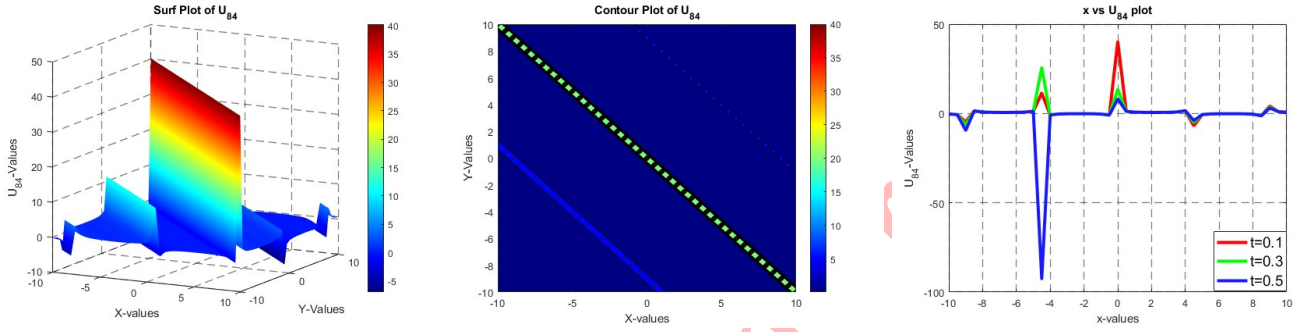


(d) 3D plot




(e) Contour plot




(f) 2D plot

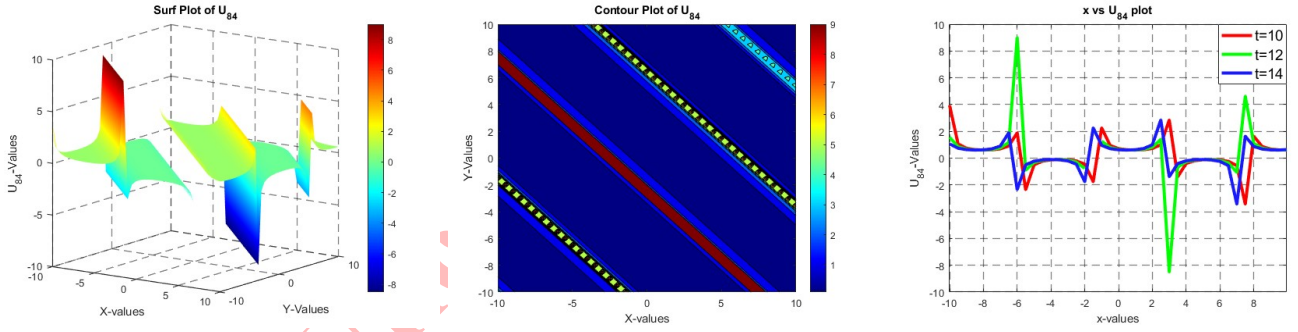


(g) 3D plot




(h) Contour plot




(i) 2D plot

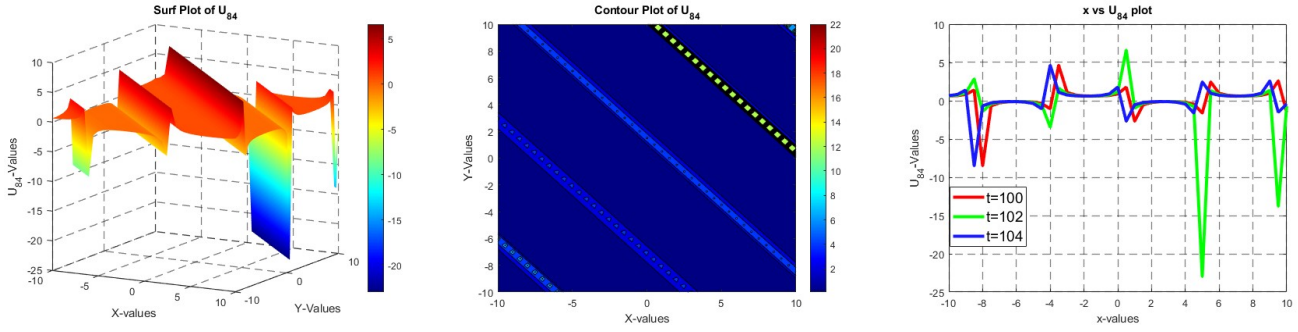


(j) 3D plot




(k) Contour plot




(l) 2D plot

**Figure 7.** Shapes for the Equation (3.47).

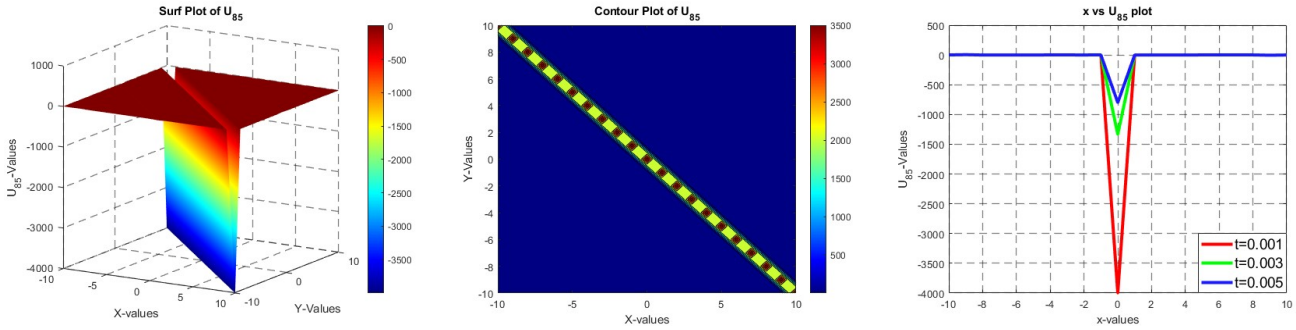


**(a)** 3D plot **(b)** Contour plot **(c)** 2D plot

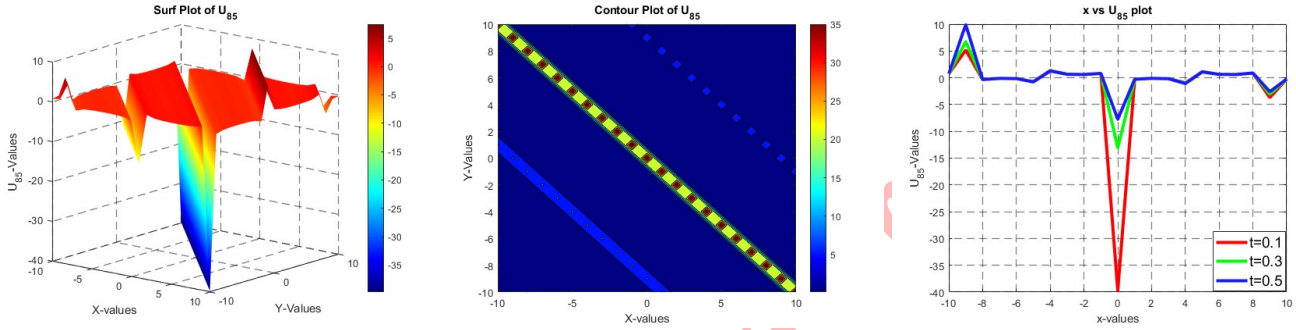


**(d)** 3D plot **(e)** Contour plot **(f)** 2D plot

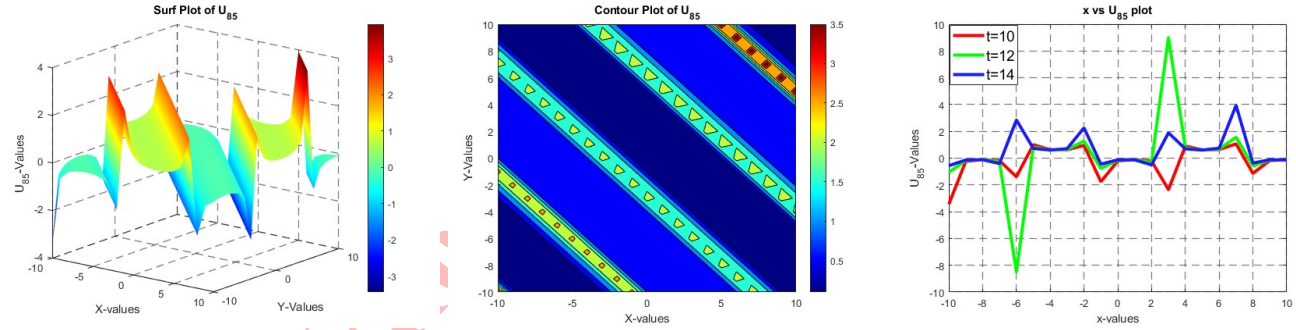


**(g)** 3D plot **(h)** Contour plot **(i)** 2D plot

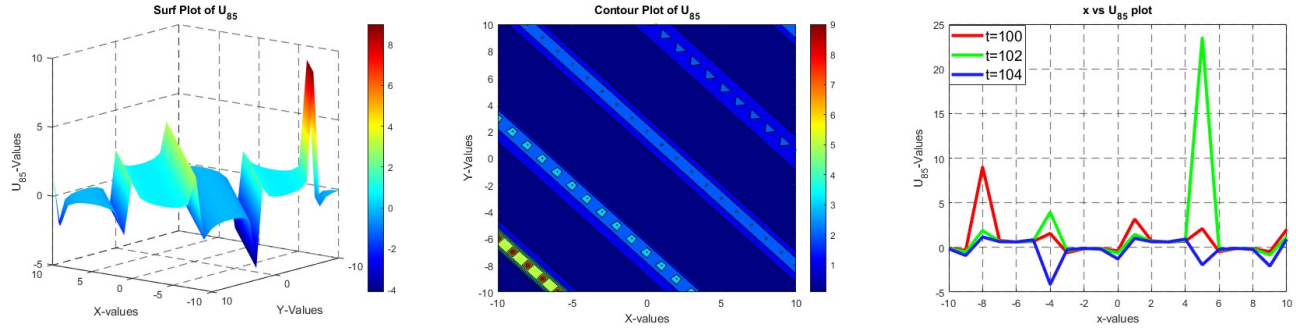


**(j)** 3D plot **(k)** Contour plot **(l)** 2D plot

**Figure 8.** Shapes for the Equation (3.48).

reveals distinct dynamic behaviors of the model, as depicted in Figures 1-8. These figures provide a comprehensive understanding of well-defined regions within nonlinear partial differential equations (NLPDEs). One of the significant advantages of this approach is its ability to generate solutions more rapidly compared to alternative methods, making it a highly efficient tool in this field. The $mG'/GE$ process is not only stable and efficient but also yields unique exact solutions that contribute to the broader understanding of NLPDEs. These solutions are valuable for advancing the study of NLPDEs, and our future work will explore further extensions of this technique to other related problems. It's important to recognise some limitations, even though the study effectively uses the $mG'/GE$ expansion method to find and analyse several correct soliton solutions of the nonlinear Jaulent–Miodek hierarchy equation. Based on idealised assumptions and precise solutions, the study is entirely theoretical. Dissipative effects, external forces, and perturbations that could occur in real-world physical systems are not considered by the model. Furthermore, the stability and interaction dynamics of the derived solutions remain unexplored. To improve the relevance in real-world scenarios, future studies may tackle these problems by experimental validation, perturbation analysis, or numerical simulations.

## Acknowledgment

**Funding:** There is no funding for this research.
**Data Availabilit:** Not applicable.
**Conflict of Interest:** No potential conflict of interest was reported by the authors.



## References

[1] S. Ahmed, B. S. T. Alkahtani, and S. S. Alzaid, *Wave propagation and soliton behaviors for the strain equation by using the sub-ODE method and expansion technique*, Int. J. Appl. Comput. Math., *10* (2024), 122.
[2] A. N. Akkilic, T. A. Sulaiman, A. P. Shakir, H. F. Ismael, H. Bulut, N. A. Shah, and M. R. Ali, *Jaulent-Miodek evolution equation: Analytical methods and various*, Results Phys., *47* (2023), 106351.
[3] G. Akram, M. Sadaf, S. Arshed, R. Latif, M. Inc, and A. S. M. Alzaidi, *Exact traveling solutions of (2+1)-dimensional extended Calogero-Bogoyavlenskii-Schiff equation using extended trial equation method and modified auxiliary equation method*, Opt. Quantum Electron., *56* (2024), 424.
[4] M. N. Alam, H. S. Akash, U. Saha, M. S. Hasan, M. W. Parvin, and C. Tunç, *Bifurcation analysis and solitary wave analysis of the nonlinear fractional soliton neuron model*, Iran. J. Sci., *47* (2023), 1797–1808.
[5] M. N. Alam, *An analytical technique to obtain travelling wave solutions to nonlinear models of fractional order*, Partial Differ. Equ. Appl. Math., *8* (2023), 100533.
[6] M. N. Alam, I. Talib, and C. Tunç, *The new soliton configurations of the 3D fractional model in arising shallow water waves*, Int. J. Appl. Comput. Math., *9* (2023), 75.
[7] M. N. Alam, H. S. Akash, U. Saha, M. S. Hasan, M. W. Parvin, and C. Tunç, *Bifurcation Analysis and Solitary Wave Analysis of the Nonlinear Fractional Soliton Neuron Model*, Iran. J. Sci., *47* (2023), 1797–1808.
[8] M. N. Alam, O. A. Ilhan, H. S. Akash, and I. Talib, *Bifurcation analysis and new exact complex solutions for the nonlinear Schrödinger equation with cubic nonlinearity*, Opt. Quantum Electron., *56* (2024), 302.
[9] W. Albalawi, N. Raza, S. Arshed, M. Farman, K. S. Nasir, and A. H. A. Abdel-Aty, *Chaotic behavior and construction of a variety of wave structures related to a new form of generalized q-Deformed sinh-Gordon model using couple of integration norms*, Math., *9*(4) (2024), 9536–9555.
[10] A. A. Ali, M. N. Alam, and M. W. Parven, *Unveilling optical soliton solutions and bifurcation analysis in the space-time fractional Fokas-Lenells equation via SSE approach*, Sci. Rep., *14* (2024), 2000.
[11] I. Alraddadi, M. A. Chowdhury, M. S. Abbas, K. EI-Rashidy, J. R. Borhan, M. M. Miah, and M. Kanan, *Dynamical Behaviors and Abundant New Soliton Solutions of Two Nonlinear PDEs via an Efficient Expansion Method in Industrial Engineering*, Math., *12*(13) (2024), 2053.
[12] S. Alshammari, M. M. A. Sawalha, and R. Shah, *Approximate analytical methods for fractional–order nonlinear system of Jaulent-Miodek equation with the Energy-Dependent Schrödinger Potential*, Fractal Fract., *7* (2023), 140.

[13] A. A. B. M. Alzahrani, *Numerical analysis of nonlinear fractional system of Jaulent-Miodek equation*, Symmetry, *15*(7) (2023), 1350.
[14] F. Badshah, K. U. Tariq, H. Ilyas, and R. N. Tufail, *Soliton, lumps, stability analysis and modulation instability for an extended (2+1)-dimensional Boussinesq model in shallow water*, Chaos Solitons Fractals, *187* (2024), 115352.
[15] F. Carbone, M. Piersanti, F. Lepreti, L. Primavera, C. N. Gencarelli, N. Pirrone, and R. Battiston, *Nonlinear shallow water investigation of atmospheric disturbances generated by strong seismic events*, Phys. Rev. E, *108* (2023), 035105.
[16] S. A. Durmus, N. Ozdemir, A. Secer, M. Ozisik, and M. Bayram, *Examination of optical soliton solutions for the perturbed Schrödinger–Hirota equation with anti-cubic law in the presence of spatiotemporal dispersion*, Eur. Phys. J. Plus, *139* (2024), 464.
[17] S. A. Fengen and H. A. Yasser, *Study of soliton interaction in optical fibers with third order dispersion and higher order nonlinear effects*, Univ. of Thi-Qar J. Sci., *10*(2) (2023), 216–223.
[18] A. H. Ganie, L. H. Sadek, M. M. Tharwat, M. A. Iqbal, M. M. Miah, M. M. Rasid, and M. S. Osman, *New investigation of the analytical behaviors for some nonlinear PDEs in mathematical physics and modern engineering*, Partial Differ. Equ. Appl. Math., *9* (2024), 100608.
[19] J. M. Heris and M. Mehrdad, *Exact Solutions for the Integrable Sixth-Order Drinfeld-Sokolov-Satsuma-Hirota System by the Analytical Methods*, Int. Scholarly Res. Notices, *2014* (2014), 840689.
[20] J. Hu and J. Qi, *Further Results about Seeking for the Exact Solutions of the Nonlinear (2+1)-Dimensional Jaulent-Miodek Equation*, Adv. Math. Phys., *2021* (2021), Article ID 5258692, 14 pages.
[21] M. Iqbal, M. N. Alam, D. Lu, A. R. Seadawy, N. E. Alsubaie, and S. Ibrahim, *Applications of nonlinear longitudinal wave equation with periodic optical solitons wave structure in magneto electro elastic circular rod*, Opt. Quantum Electron., *56* (2024), 1031.
[22] M. Iqbal, M. N. Alam, D. Lu, A. R. Seadawy, N. E. Alsubaie, and S. Ibrahim, *On the exploration of dynamical optical solitons to the modify unstable nonlinear Schrödinger equation arising in optical fibers*, Opt. Quantum Electron., *56* (2024), 765.
[23] M. Iqbal, A. R. Seadawy, D. Lu, and Z. Zhang, *Physical structure and multiple solitary wave solutions for the nonlinear Jaulent-Miodek Hierarchy equation*, Mod. Phys. Lett. B, *38*(16) (2024), 2341016.
[24] M. Iqbal, A. R. Seadawy, D. Lu, and Z. Zhang, *Physical structure and multiple solitary wave solutions for the nonlinear Jaulent-Miodek Hierarchy equation*, Mod. Phys. Lett. B, *38*(16) (2024), 2341016.
[25] D. Kaya and S. M. E. Sayed, *A numerical method for solving Jaulent-Miodek equation*, Phys. Lett. A, *318*(4-5) (2003), 345–353.
[26] J. Manafian, M. Lakestani, and A. Bekir, *Comparison between the generalized tanh-coth and the $(G'/G)$-expansion methods for solving NPDEs and NODEs*, Pramana J. Phys., *87* (2016), 95.
[27] J. Muhammad, M. B. Riaz, U. Younas, N. Nasreen, A. Jhangeer, and D. Lu, *Extraction of Optical wave structures to the coupled fractional system in magneto-optic waveguides*, Arab J. Basic Appl. Sci., *31*(1) (2024), 242–254.
[28] W. B. Rabie, H. M. Ahmed, M. S. Hashemi, M. Mirzazadeh, and M. Bayram, *Generating optical solutions in the extended (3+1)-dimensional nonlinear Kudryashov's equation using the extended F-expansion method*, Opt. Quantum Electron., *56* (2024), 894.
[29] W. B. Rabie, T. A. Khalil, N. Barda, H. M. Ahmed, M. Mirzazadeh, and M. S. Hashemi, *Soliton solutions and other solutions to the (4+1)-dimensional Davey-Stewartson-Kaddomtsev-Petviashvili equation using modified extended mapping method*, Qual. Theory Dyn. Syst., *23* (2024), 87.
[30] M. M. Roshid, M. N. Alam, O. A. İlhan, M. A. Rahim, M. M. H. Tuhin, and M. M. Rahman, *Modulation instability and comparative observation of the effect of fractional parameters on new optical soliton solutions of the paraxial wave model*, Opt. Quantum Electron., *56* (2024), 1010.
[31] R. Sadat and M. Kassem, *Explicit solutions for the (2+1)-dimensional Jaulent-Miodek equation using the integrating factors method in an unbounded domain*, Math. Comput. Appl., *23*(1) (2018), 15.
[32] S. Sahoo and S. S. Ray, *New solitary wave solutions of time-fractional coupled Jaulent-Miodek equation by using two reliable methods*, Nonlinear Dyn., *85* (2016), 1167–1176.

[33] S. Sahoo, S. S. Ray, M. A. M. Abdou, M. Inc, and Y. M. Chu, *New soliton solutions of fractional Jaulent-Miodek system with symmetry analysis*, Symmetry, *12*(6) (2020), 1001.

[34] Y. Shen, B. Tian, and T. Y. Zhou, *Studies on an extended (3+1)-dimensional variable-coefficient shallow water wave equation: Bilinear form, Pfaffian solutions and Solitonic interactions*, Appl. Comput. Math. Int. J., *23*(1) (2024), 40–52.

[35] W. M. Taha and M. S. M. Noorani, *Exact solutions of equation generated by the Jaulent-Miodek Hierarchy by* $(G'/G)$*-expansion method*, Math. Probl. Eng., *2013* (2013), Article ID 392830, 1–7.

[36] K. U. Tariq, A. Bekir, S. Nisar, and M. Alp, *Construction of new wave structures and stability analysis for the nonlinear Klein-Gordon equation*, Phys. Scr., *99* (2024), 055220.

[37] S. W. Yao, M. E. Islam, M. A. Akbar, Inc. Mustafa, M. Adel, and M. S. Osman, *Analysis of parametric effects in the wave profile of the variant Boussinesq equation through two analytical approaches*, Open Phys., *20*(1) (2022), 778–794.

[38] J. Zhang, J. Manafian, S. Raut, S. Roy, K. H. Mahmoud, and A. S. A. Alsubaie, *Study of two soliton and shock wave structures by weighted residual method and Hirota bilinear approach*, Nonlinear Dyn., *112* (2024), 12375–12391.